

# Three-component seismic data processing: Carrot Creek, Alberta

Mark P. Harrison

## ABSTRACT

A survey using three-component geophones to record seismic reflection data from a vibrator source was conducted in the Carrot Creek area of Alberta. Two lines were recorded in total, each having components in the vertical, radial, and transverse directions.

This report outlines the data-processing sequence that is currently being used for converted-wave analysis using the CREWES data processing centre. In particular, results are shown for the vertical (P-wave) and radial (SV-wave) components of line CC-SW-01 of the Carrot Creek survey.

Little reflection signal was seen on the transverse component records. This suggests that any velocity anisotropy in the area is either small enough to neglect, or the line orientation relative to the direction of anisotropy gives negligible rotation of SV shear energy propagating in the line plane.

It was found in processing the radial-component data that the source static solution obtained from the vertical component processing was appropriate for the converted shear data. The vertical component receiver statics, however, were not able to properly correct the radial component receivers. From common-receiver surface stacks, short wavelength residual statics as high as 60 ms were seen to remain in the radial component data. There appears to be little correlation between the size and location of static pockets found on the radial component data to those found on the vertical component data.

Processing of the radial component data set resulted in a stacked section for the converted-wave shear energy. Enough signal strength exists to allow the correlation of events between the P-P and P-SV sections, allowing the rough computation of average  $V_p/V_s$  ratios between events.

The target in this area is the oil-bearing Cardium formation, which is a thin Upper Cretaceous sandstone and conglomerate. A pronounced brightening is seen to occur on the SV-wave section at two locations on the line, both of which correspond to known pools. Little amplitude change is visible on the P-wave section at these locations.

## INTRODUCTION

Different rock types having the same sonic velocities and surrounded by the same lithology will produce seismic reflection responses that are virtually identical. This makes the task of trying to distinguish between potential rock-types based on conventional reflection data alone extremely difficult, if not impossible. It has been suggested by Pickett (1963) and others more recently that Poisson's ratio might be able to provide a way of discriminating between rock types which have very similar compressional velocities. Poisson's ratio itself is only a function of the ratio of shear-wave and compressional-wave velocities. A method which would enable us to compute this ratio would allow us to compute Poisson's ratio, from which we might better be able to infer rock type.

Compressional waves striking a reflecting boundary in an elastic media at non-zero angles of incidence can give rise to both reflected and transmitted shear waves through mode conversion. These shear waves are vertically polarized relative to the reflecting surface, and are commonly known as SV waves. The amount of conversion that occurs is dependent on both the angle-of-incidence and the rock properties at the reflecting interface (see Aki and Richards, 1980). The transfer of energy from compressional to shear at non-normal incidence angles leads to predictable changes in the compressional reflection coefficient with offset.

In the absence of layer dip and velocity anisotropy, the converted SV-waves will emerge at the surface as nearly horizontal oscillations oriented in the inline-direction (see Douma and Helbig, 1987, for discussion). Because geophones used in conventional shooting record only the vertical component of ground movement, the mode-converted shear data are largely lost.

Seismic surveys are currently being conducted that make use of geophones capable of sensing motion in the horizontal directions as well as the vertical, giving rise to multi-component data sets for each shot record. This allows the recording and analysis of any converted-wave shear data that might have been generated by the sub-surface geology.

If any usable amount of converted-wave shear data can actually be recorded at the surface, then processing and analysis of this data, combined with the processed compressional-wave data, might enable us to determine the compressional-to-shear velocity ratio  $V_p/V_s$ . This, in turn, would enable the direct calculation of Poisson's ratio.

This report outlines the sequence that was used in the processing of a multi-component vibrator line acquired in the Carrot Creek area. The target in this area is the Upper Cretaceous Cardium formation, which is a thin sandstone and conglomerate. Figure 1 shows the location and orientation of the line, which is seen to cross two known Cardium pools as outlined by Joiner (1989).

In this survey geophone motion was recorded in the three following directions for each source point;

- 1) the vertical direction
- 2) the radial (inline-horizontal) direction
- 3) the transverse (crossline-horizontal) direction

Because of the low velocity of the weathered surface layer, the normal to the reflected and converted wavefronts emerging from the ground at the geophones should be near-vertical. This places the compressional (P) energy on the vertical channel, and the converted shear (SV) energy on the horizontal channels. The layer interfaces in this area are nearly flat, which should put the bulk of the SV energy on the radial channel in the absence of anisotropic velocity effects.

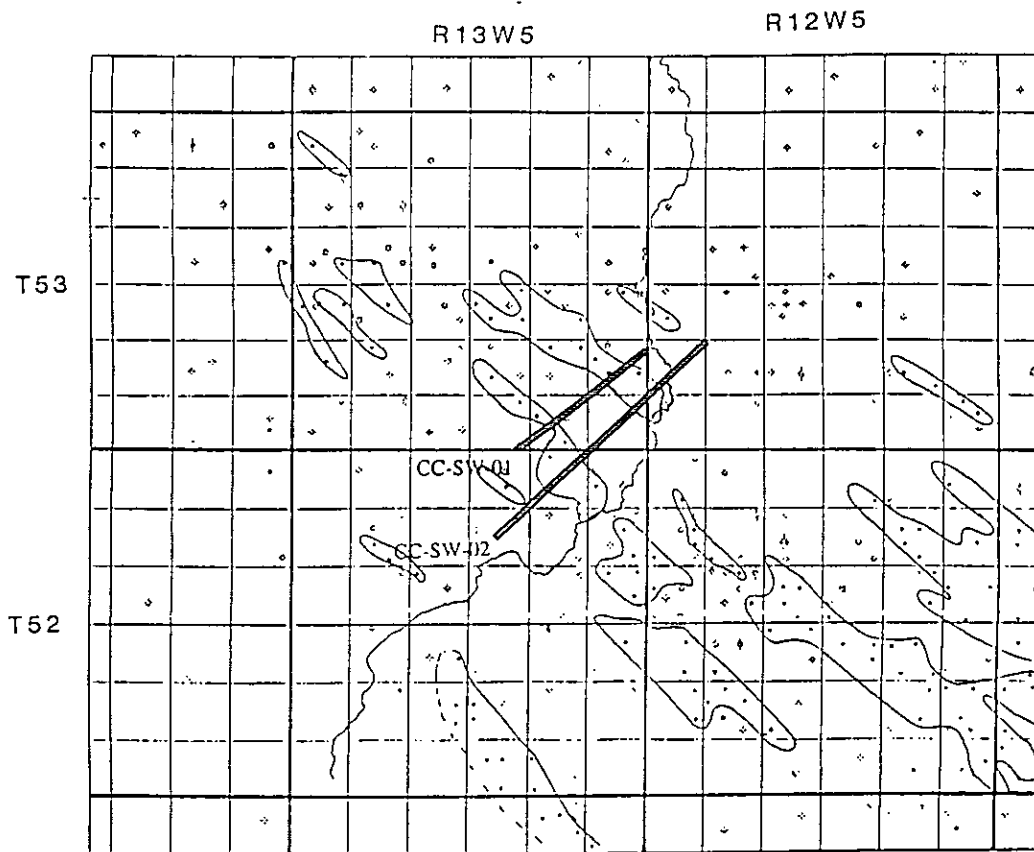


Figure 1. Location of lines CC-SW-01 and CC-SW-02 in the Carrot Creek Survey.

## METHOD

Table 1 gives a summary of the field data acquisition parameters. The survey was carried out using a vibrator source and a 240-trace recording system. All three geophone directional components were recorded on the same amplifier, resulting in data collection from 80 receiver stations for each source point. Each receiver station consisted of a single 3-directional geophone. No data were recorded at source-to-receiver offsets less than 180 meters (6 groups), and the normal cable recording arrangement gives a maximum offset of slightly over 2.5 km.

Figure 2 shows the data recorded in the vertical direction for source points located at approximately one-third and two-thirds of the distance down the line. Figures 3 and 4 show the data recorded in the radial and transverse directions for the same two source points. A time-variant gain function followed by individual trace-balance scaling has been applied to the field records to compensate for geometric spreading and field gain. The time scale for the horizontal component data on these and all following plots has been adjusted to be two-thirds of that of the vertical component displays. The  $V_p/V_s$  ratio for most rock types is in the neighbourhood of 2.0 (see Tatham, 1985), so that plotting the converted-wave data at this reduced time scale will allow us to more easily correlate between the compressional and converted shear data sets.

Table 1. Field acquisition and recording parameters for line CC-SW-01 of the Carrot Creek survey.

Energy source	Vibroseis
Number of vibrators used	4
Number of sweeps per VP	10
Source pattern length	30 meters
Sweep frequency	10-94 hz
Sweep length & type	6 second linear
Amplifier type	Sercel SN348
Number of channels	240
Sample rate	2 ms
Low-cut filter	Out
Antialias filter	125 hz
Notch filter	Out
Geophones per group	1
Type of geophones used	LRS 1033, 10 hz
Number of groups recorded	80
Group interval	30 meters
Normal source interval	60 meters

All three components show a low-velocity noise-train originating from the source that travels with a velocity of about 340 m/s, which is very close to the speed of sound in air. This strongly suggests that the noise-train is associated with an air-wave from the vibrators. The radial component data records have a second noise-train traveling with a horizontal velocity of about 1280 m/s that is not present on the vertical channel. Ground roll radiating away from the source would give particle motion at the surface in both the vertical and horizontal directions, which doesn't appear to be the case here. Love waves generated by the source should give particle motion in the transverse direction rather than the inline direction (Aki and Richards, 1980), which eliminates them as the noise train propagator. The presence of the noise train on the radial channel coupled with its velocity would then suggest that it might be refracted shear energy that has been generated by the vibrators. The ratio of the P-wave refraction velocity of 3150 m/s to the noise-train velocity gives a  $V_p/V_s$  ratio of 2.46, which is reasonable for a loosely-consolidated near-surface (Garotta, 1985). A comparison of the P and SV event times for a shallow marker on the final processed sections suggest an average  $V_p/V_s$  ratio of 2.57 for the first roughly 350 meters of depth, which is supportive.

The radial component is seen to have good signal strength, with events that roughly correspond to those on the vertical channel. It is possible to see the polarity reversal between the receivers on the left and those on the right on the split-spread raw record. The transverse component, however, is seen to have almost no recognizable reflection signal, and has not been processed any further.

The vertical channel data was processed using the conventional P-wave processing flow outlined in Table 2. The vibrator records were picked for best-guess arrival times, from which layer replacement statics were computed. Geometric spreading compensation

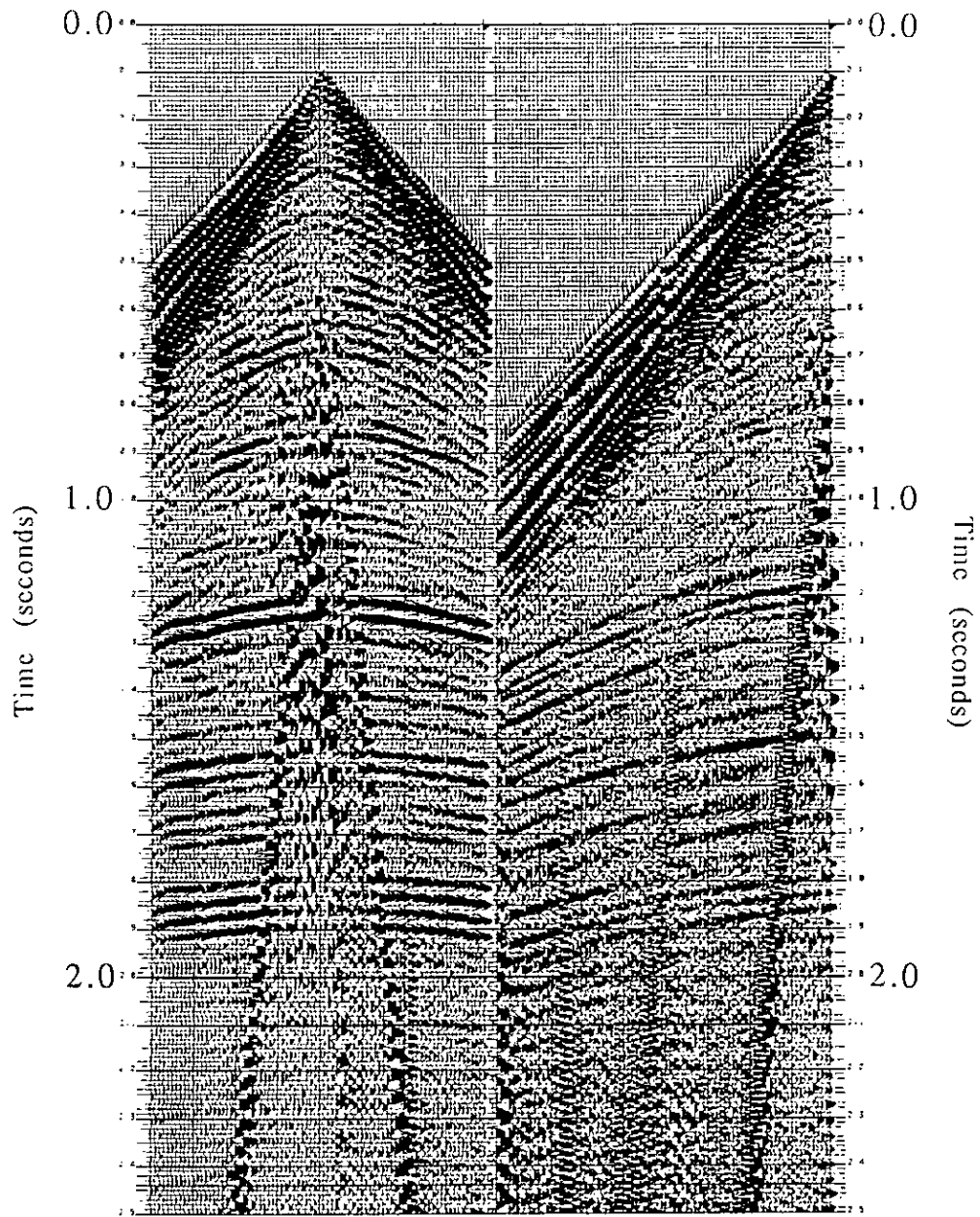


Figure 2. Data recorded in the vertical direction for VP's 115 and 211.

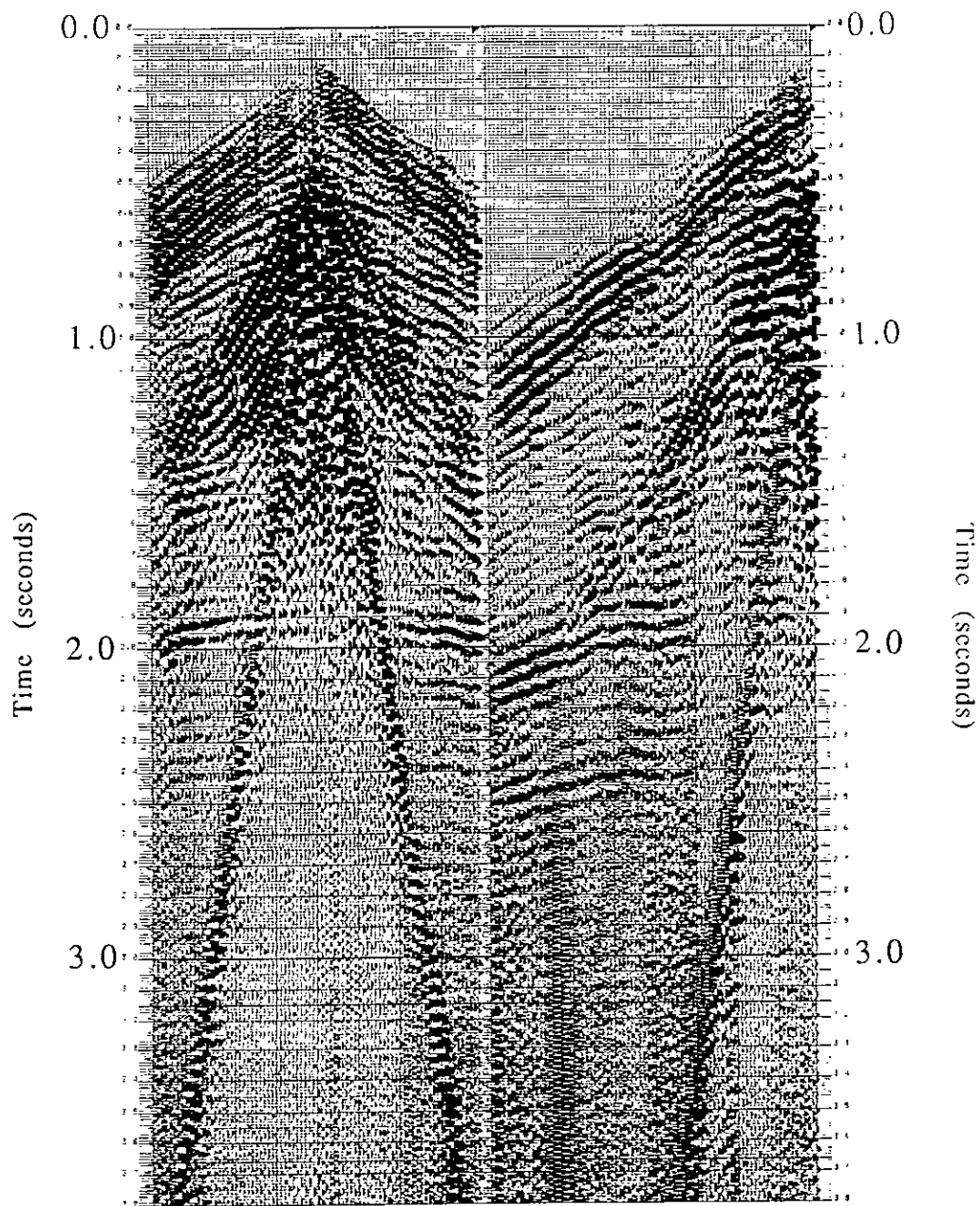


Figure 3. Data recorded in the radial direction for VP's 115 and 211.

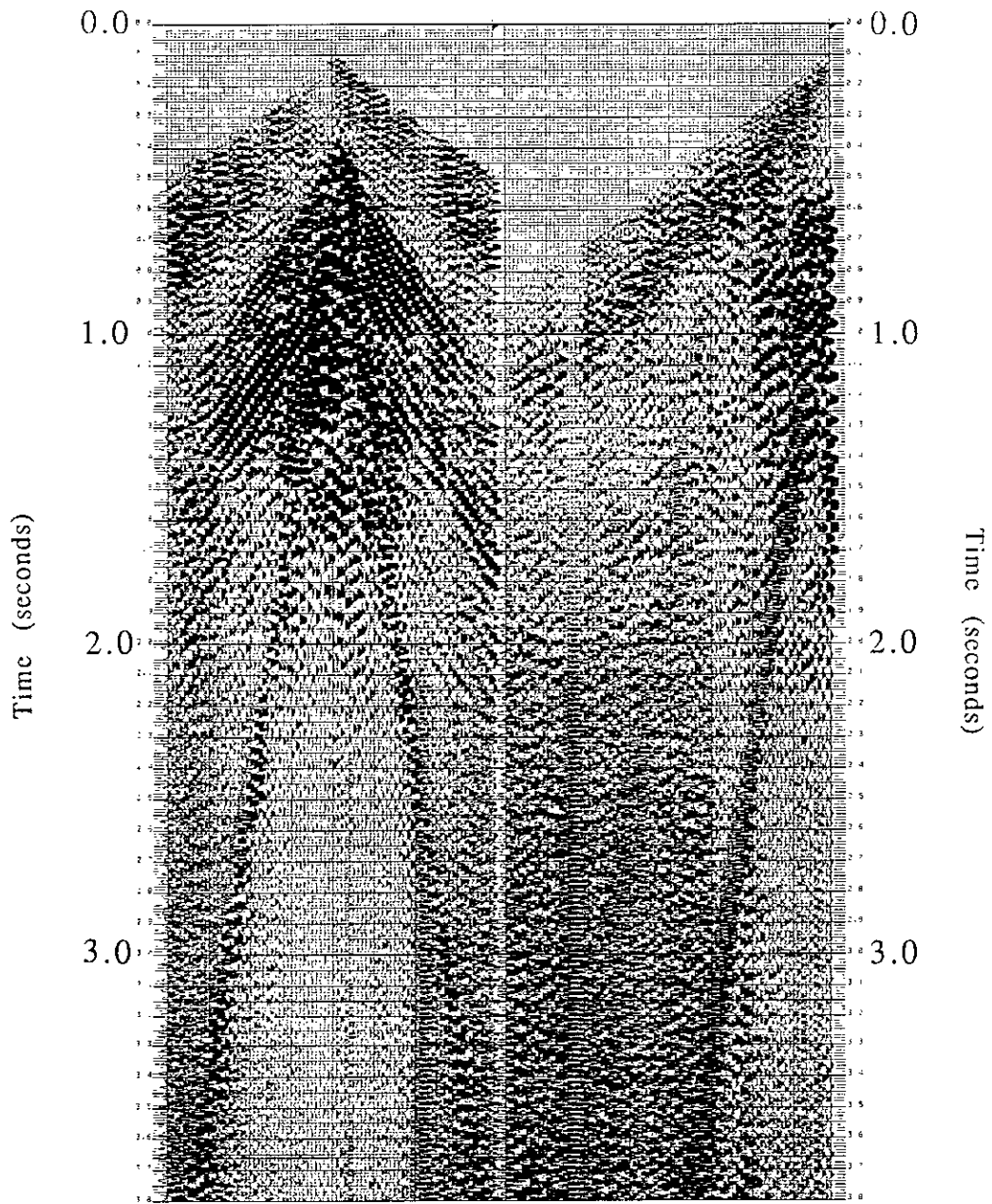


Figure 4. Data recorded in the transverse direction for VP's 115 and 211.

Table 2. Processing sequence and parameters for the vertical channel data.

DEMULTIPLEX  
 GEOMETRIC SPREADING COMPENSATION  
 SPIKING DECONVOLUTION  
     80 ms operator, 0.1% prewhitening  
 CDP SORT  
 APPLY ELEVATION & REFRACTION STATICS  
 INITIAL VELOCITY ANALYSIS  
 AUTOMATIC SURFACE-CONSISTENT STATICS  
     Correlation window from 300 to 2050 ms  
     Maximum shift of + or - 16 ms  
 VELOCITY ANALYSIS  
 NORMAL MOVEOUT APPLICATION  
 MUTE  
 CDP TRIM STATICS  
     Correlation window from 250 to 2050 ms  
     Maximum shift of + or - 10 ms  
 STACK  
 BANDPASS FILTER  
     Zero-phase, 14-70 hz  
 RMS GAIN  
     First window of 200 ms, second of 400 ms,  
     subsequent windows of 800 ms length.

was applied using the formula given by Newman (1973);

$$\text{Gain (t)} = \frac{tV^2}{V_1}$$

where t is the two-way time, V is the RMS stacking velocity, and  $V_1$  is the velocity of the first layer.

The final stack section is displayed in Figure 5 with the north-east side on the right, and, as a whole, is of very good quality. The shallower part of the section is a little noisy, possibly because of the smaller amount of noise attenuation provided by single geophones. A mild f-k filter with a pass-band from -2 to +2 ms/trace and a 6 db maximum reject was applied to the section to give the result shown in Figure 6. A plot of the average time-variant cross-power spectra between adjacent stack traces is shown in Figure 7. This plot indicates that we have a usable bandwidth from approximately 10-55 hz, with little depth dependence (basement is at around 1900 ms).

The Cardium event is located at a time of about 990 ms on the section, and does not show any obvious amplitude change at the location of the two pools.

The radial (P-SV) component was processed using the sequence shown in Table 3. Geometric spreading compensation was applied using a formula derived from arguments similar to those of Newman (1973);

$$\text{Gain (t)} = \frac{tV^2}{V_1}$$

where t is the two-way time, V is the converted-wave stacking velocity, and  $V_1$  is the compressional velocity of the first layer.

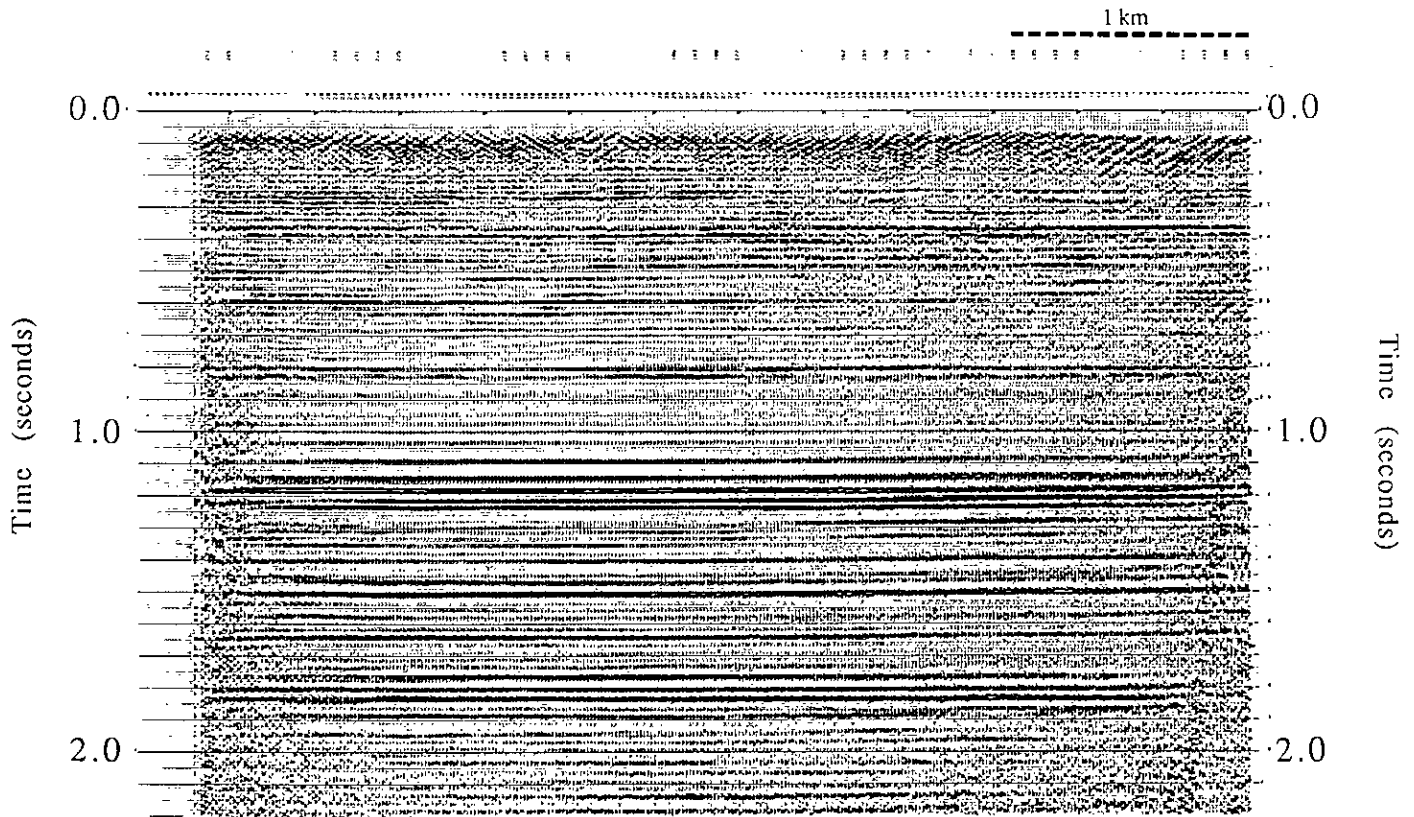


Figure 5. Final stack section for the vertical (P-P) component data.

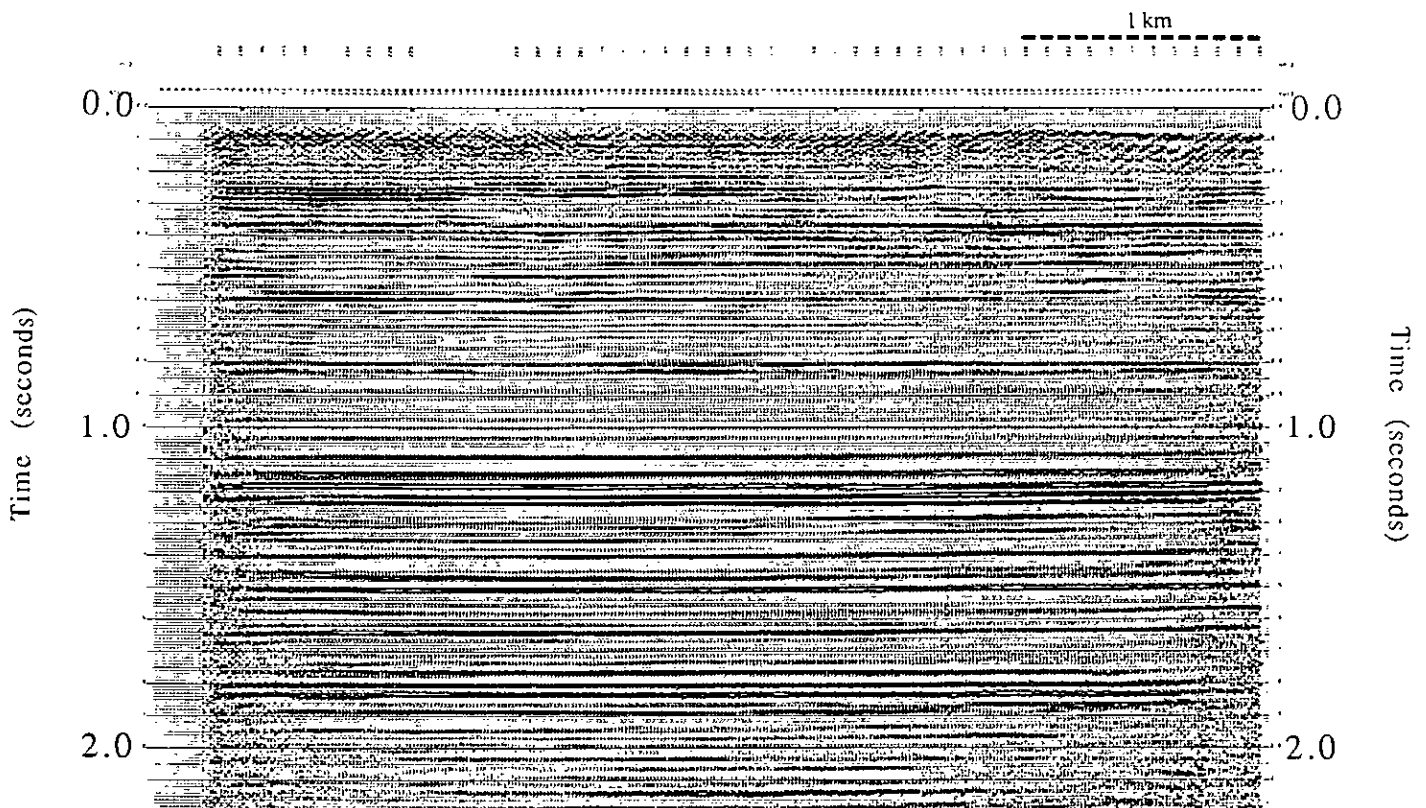
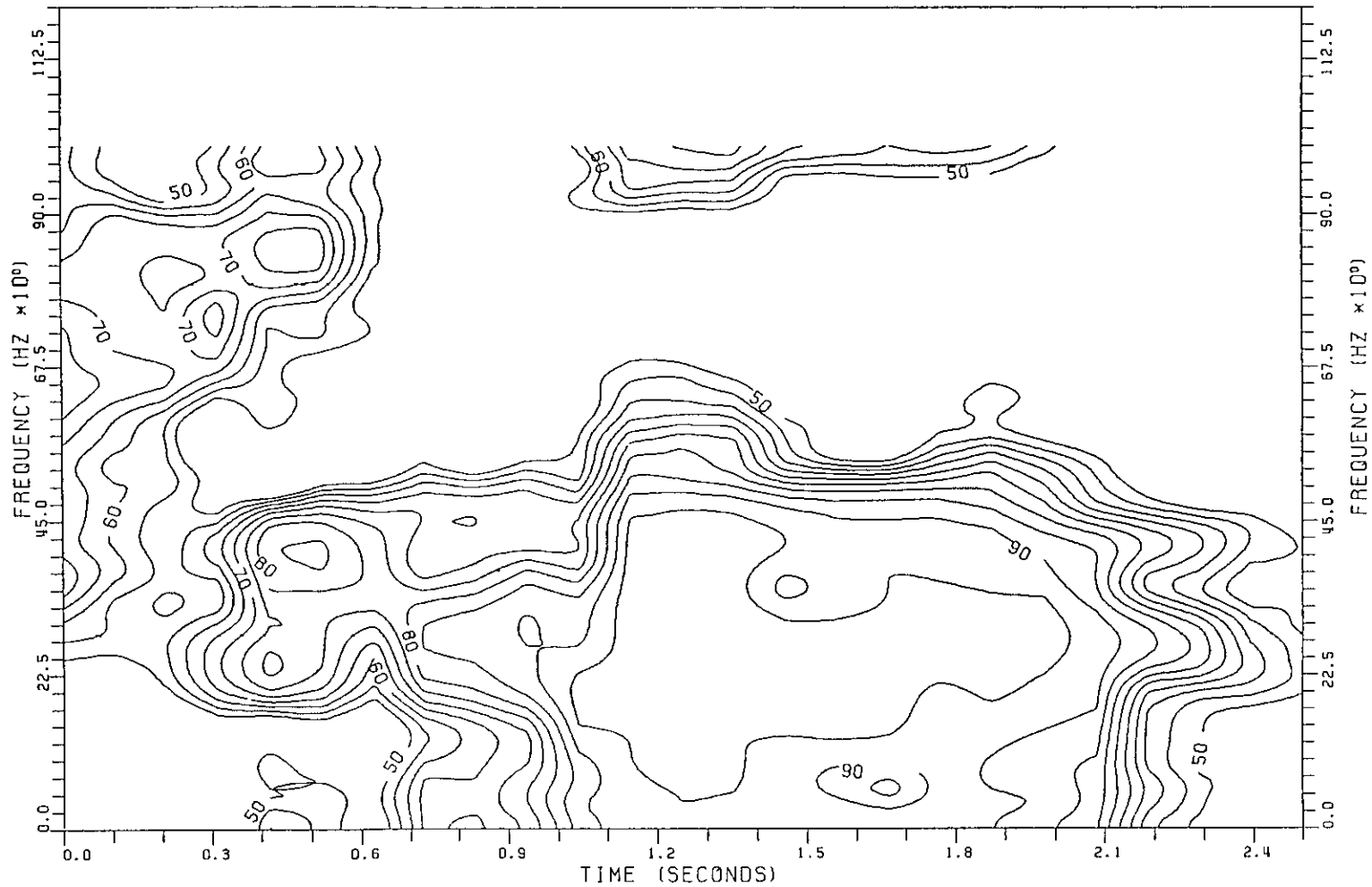


Figure 6. F-K filter applied to the final stack section for the vertical (P-P) component data.

SPECTRA AVERAGED OVER 20 CALCULATIONS  
ENDING WITH IDENT 50000 TRACE 21

MAXIMUM = 0.9870E0



CARROT CREEK CCSW01 (VERTICAL)  
WINDOW LENGTH = 400 (MS) WINDOW ADVANCE = 100 (MS) STARTING TIME = 0 (MS)  
CONTOURS ARE OF SMOOTHED COHERENCE SPECTRA IN PERCENT

Figure 7. Average time-variant cross-power spectrum between adjacent stack traces of the vertical (P-P) component data.

Table 3. Processing sequence and parameters for the radial (P-SV) channel data.

DEMULPLEX  
GEOMETRIC SPREADING COMPENSATION  
SPIKING DECONVOLUTION  
    120 ms operator, 0.1% prewhitening  
REVERSE THE POLARITY OF TRAILING SPREAD  
APPLY FINAL P-WAVE STATICS  
INITIAL VELOCITY ANALYSIS  
APPLY HAND STATICS FROM SURFACE STACKS  
AUTOMATIC SURFACE-CONSISTENT STATICS  
    Correlation window from 400 to 2600 ms  
    Maximum shift of + or - 18 ms  
CDP STACK  
CONVERTED-WAVE REBINNING  
    Vp/Vs ratio of 1.95 used  
VELOCITY ANALYSIS  
NORMAL MOVEOUT APPLICATION  
MUTE  
CDP TRIM STATICS  
    Correlation window from 400 to 3100 ms  
    Maximum shift of + or - 14 ms  
STACK  
BANDPASS FILTER  
    Zero-phase, 8-35 hz  
RMS GAIN  
    First window of 300 ms, second of 600 ms,  
    subsequent windows of 900 ms length.

In a horizontally layered medium, SV shear energy that arrives at the surface should be radially symmetric about the sourcepoint. The radial geophone sensors of receivers are pointed at the source on one side of the spread, and away from the source on the other side. This means that a converted wave from a horizontal plane in the earth gives rise to motion at the surface that is recorded as a negative voltage by one side of the spread, and as a positive voltage on the other side. This requires that we flip the polarity of one side of the spread, as is shown in Table 3.

We would expect that application of the final P-P static solution to the P-SV data would give the correct solution for the source static component. This should occur because the converted data first passes down through the surface as P-wave energy from the source, encountering the same surface conditions and delays as the vertical channel data. If this holds, then the residual statics problem should then reduce to one of having to determine only the residual receiver static. After conversion occurs at the reflecting interfaces, the signal traveling back to be recorded on the horizontal receiver component is SV shear. We would expect the near-surface delay time of the SV data to be greater than that for the P-P data by a factor roughly equal to the average Vp/Vs ratio for the near-surface, assuming that both P and SV signals see the same thicknesses of near-surface material. The P-P data for this line shows almost no short-wavelength variation in static correction, implying nearly constant layer thickness for the near-surface. If this were true for the P-SV data as well, then application of the final P-P statics to the P-SV data should leave little high-frequency static remaining.

Figure 8 shows a stack section for the P-SV data created using the final P-P static solution and the final P-SV mute and velocities determined later in the processing sequence. The reflectors are seen to be improperly stacked, strongly suggesting that we have

substantial residual static remaining. Figures 9 and 10 show common-receiver and common-source stack displays for the P-SV data that went into creating the stack in Figure 8. From these displays we see that we do still have short-wavelength residual receiver statics remaining that are as large as 60 ms. This implies that the SV data passing up through the near-surface do not see the same constant layer thicknesses as the P data, which leads to substantial static differences between the two data sets.

Residual receiver statics were picked by hand from the common-receiver stack section and applied to the data to give a second set of CMP and surface stacks. These new stacks were greatly improved over the previous set. In particular, the new common-source stack showed much greater coherency, with no visible residual source static. A pass of automatic surface-consistent residual statics was made later in the processing sequence to remove any remaining statics.

Once a reasonably good P-SV section was obtained, an average Vp/Vs ratio was determined down to the Cardium, which appears at a time of 1600 ms on the P-SV section. This was done by hand-correlating events on the P-P and P-SV sections to get event times, then using the following formula to compute a Vp/Vs ratio between events;

$$V_p/V_s = \frac{2I_s}{I_p} - 1$$

where  $I_p$  is the P-P time interval, and  $I_s$  is the P-SV time interval.

Results of these calculations are given in Table 4. An average Vp/Vs ratio down to the Cardium was calculated using the values computed between events weighed by the time

Table 4. Vp/Vs ratios computed from event and interval time for reflected (P-P) and converted (P-SV) data.

P-P time	P-P interval	P-SV time	P-SV interval	Vp/Vs
260 ms		480 ms		
	118 ms		190 ms	2.22
378 ms		670 ms		
	214 ms		330 ms	2.08
592 ms		1000 ms		
	224 ms		320 ms	1.86
816 ms		1320 ms		
	184 ms		270 ms	1.93
1000 ms	** CARDIUM **	1590 ms		
	94 ms		128 ms	1.72
1094 ms		1718 ms		
	90 ms		126 ms	1.80
1184 ms		1844 ms		
	172 ms		228 ms	1.65
1356 ms		2072 ms		
	132 ms		208 ms	2.15
1488 ms		2280 ms		
	156 ms		224 ms	1.87
1644 ms		2504 ms		
	190 ms		276 ms	1.91
1834 ms		2780 ms		

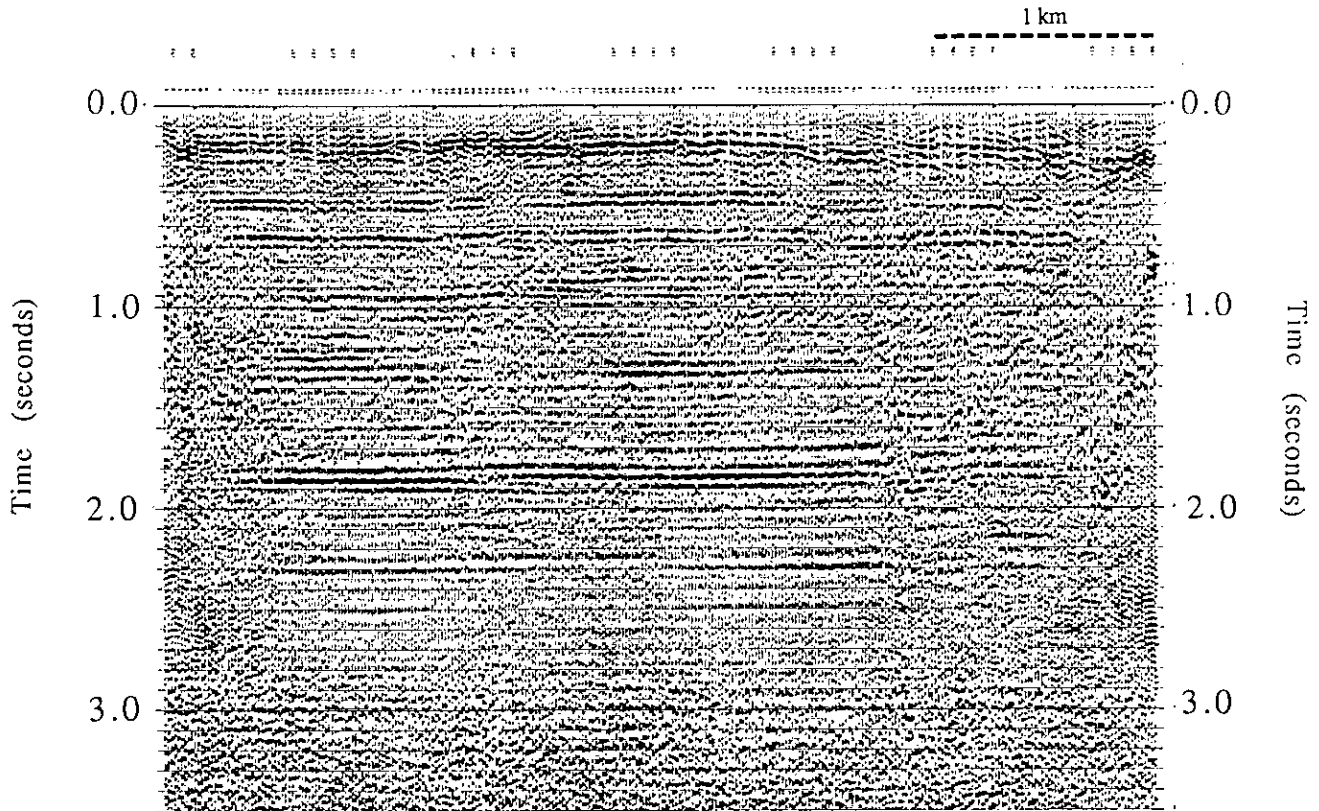


Figure 8. Stack section for the radial (P-SV) component data created using the final vertical component static solution.

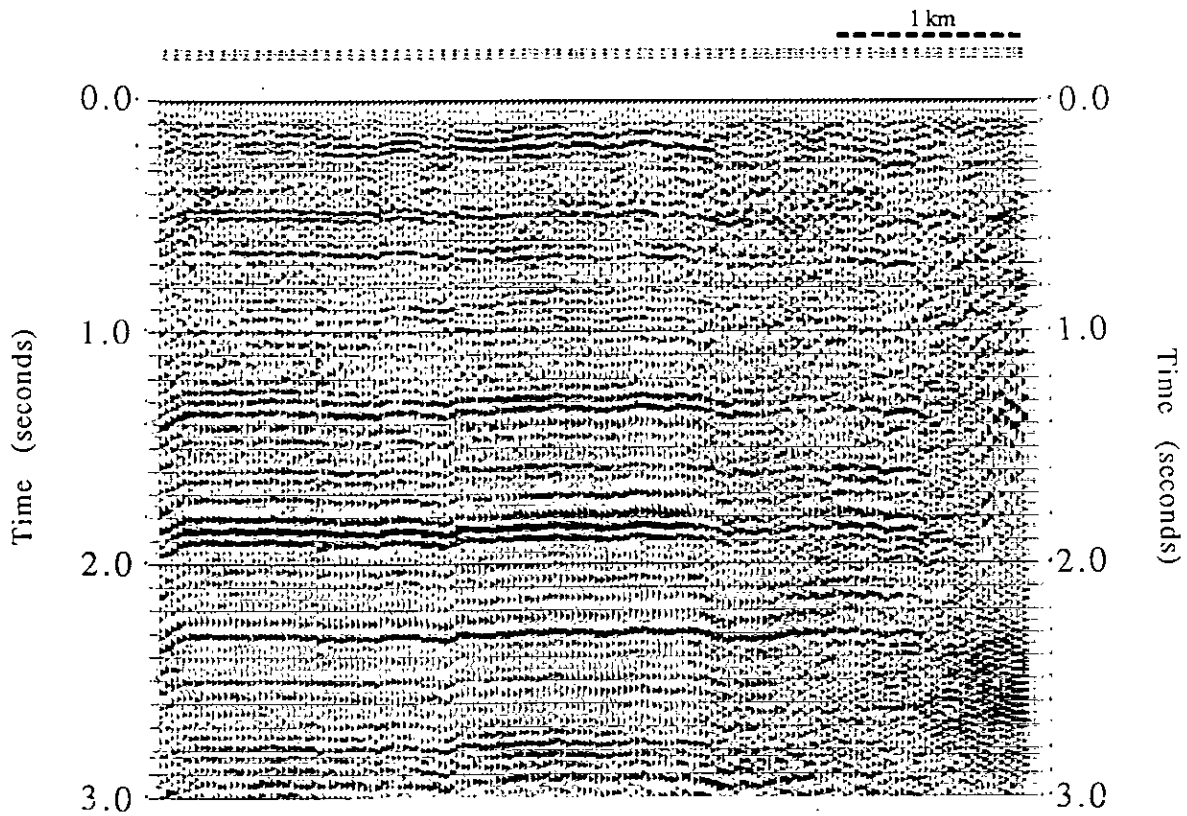


Figure 9. Common-receiver stack section for the radial (P-SV) component data with the final P-P statics applied.

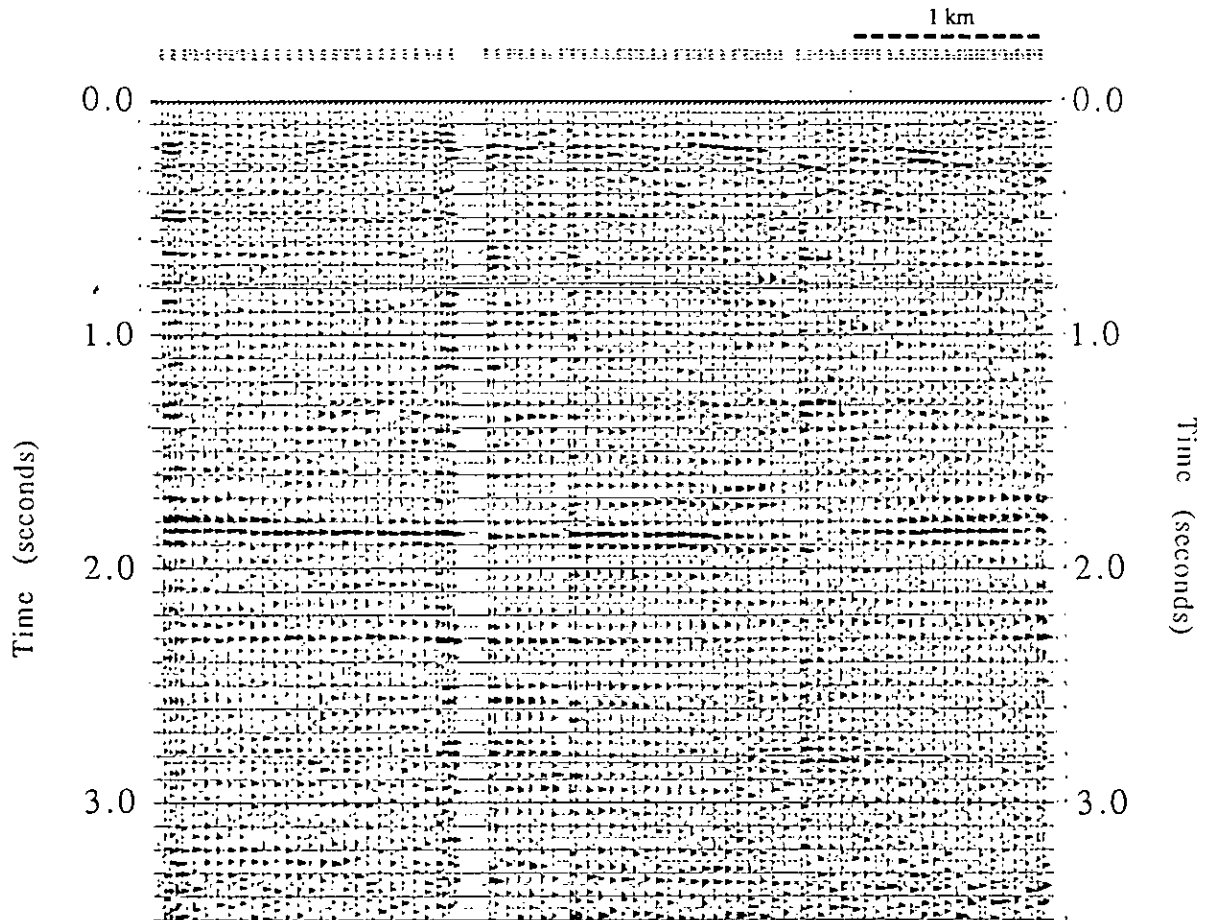


Figure 10. Common-sourcepoint stack section for the radial (P-SV) component data with the final P-P statics applied.

interval over which the value was computed. This resulted in a  $V_p/V_s$  value of 1.95 for this line.

Once the average  $V_p/V_s$  ratio was determined, the converted-wave data were rebinned using this ratio and the conversion-point formula derived by Fromm, Krey, and Wiest (1985) given below;

$$X_p = \frac{X}{1 + (V_s/V_p)}$$

where  $X$  is the total source-to-receiver offset and  $X_p$  is the offset from the source to the conversion point. This formula is a first-order approximation for a single horizontal homogenous layer. Tessmer and Behle (1988) show that this approximation can result in considerable errors in bin positioning at moderate offsets, and propose a modified formula that is more accurate. Eaton (1989) has applied this improved formula to rebin synthetic data, but his method has not yet been applied to this data volume.

Velocity analysis was done on the P-SV data using conventional hyperbolic NMO curve-fitting. Sample velocity analysis plots for each of the P-P and P-SV data sets are displayed in Figure 11. Tessmer and Behle (1988) discuss the applicability and accuracy of this method, and derive a relationship between the converted-wave stacking velocities and the compressional and shear interval velocities. Sample common-offset stack records constructed approximately in the centre of the line for each of the P-P and P-SV data sets are shown in Figure 12. The P-SV record indicates that at short offsets we get little mode conversion, and that as we move to increasing offset we get progressively more conversion, as expected from the Zoeppritz equations (see Aki and Richards, 1980). The strong event located at about 1200 ms on the P-P record suggests that we are getting measurable decreases in amplitude with offset, but no analysis has yet been done to confirm this or relate this to P-SV amplitude changes with offset.

The final P-SV stack section is displayed in Figure 13, again with the north-east side on the right. The noise level on this plot is qualitatively seen to be greater than that of the P-P section, especially at depth. A mild f-k filter with a pass-band from -3 to +3 ms/trace and a 6 db maximum reject was applied to the section to give the result shown in Figure 14. A plot of the average time-variant cross-power spectra between adjacent traces is shown in Figure 15. This plot indicates that we have a usable bandwidth from approximately 6-30 hz, with a gradual decrease in peak frequency with depth (basement is at around 3000 ms). This bandwidth is roughly half that of the P-P section.

The Cardium event is located at a time of about 1600 ms on the P-SV section, and we do see a pronounced amplitude increase at two positions on the line which correspond to the pool locations shown in Figure 1.

## DISCUSSION

Displays of the raw records indicate that we might be getting source-generated shear energy which refracts along the near-surface. Schafer (1989) gives other examples of what appear to be refracted shear energy from the source. Analysis of the travel times for this energy might enable the computation of a shear-wave near-surface thickness and velocity model from which static corrections for the converted wave data could be determined.

Common-receiver stacks produced after the application of the final P-P static solution shows that we get large residual statics that the P-P solution does not account for, implying that the SV data passing up through the near-surface does not see the same layer thicknesses as the P data. These thickness differences might be explained by the depth of the water table in this area. If this depth were nearly constant, then the P-wave energy would only see low-velocity material down to this depth. Once the water table is reached,

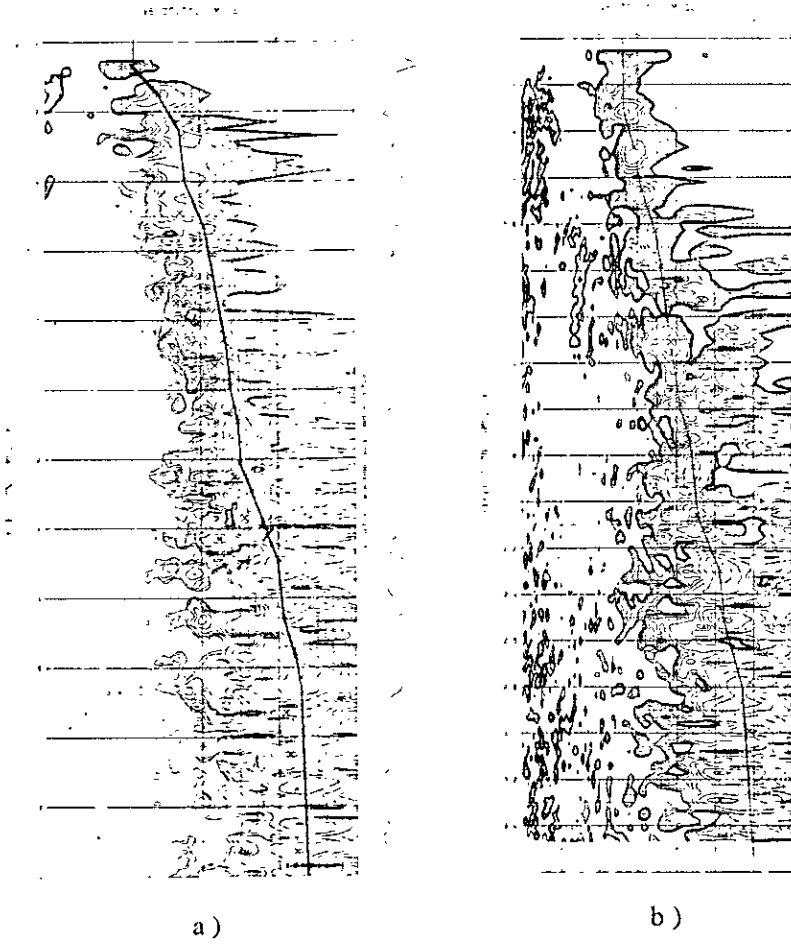


Figure 11. Sample velocity analysis plots for a) the vertical component and b) the radial component data sets.

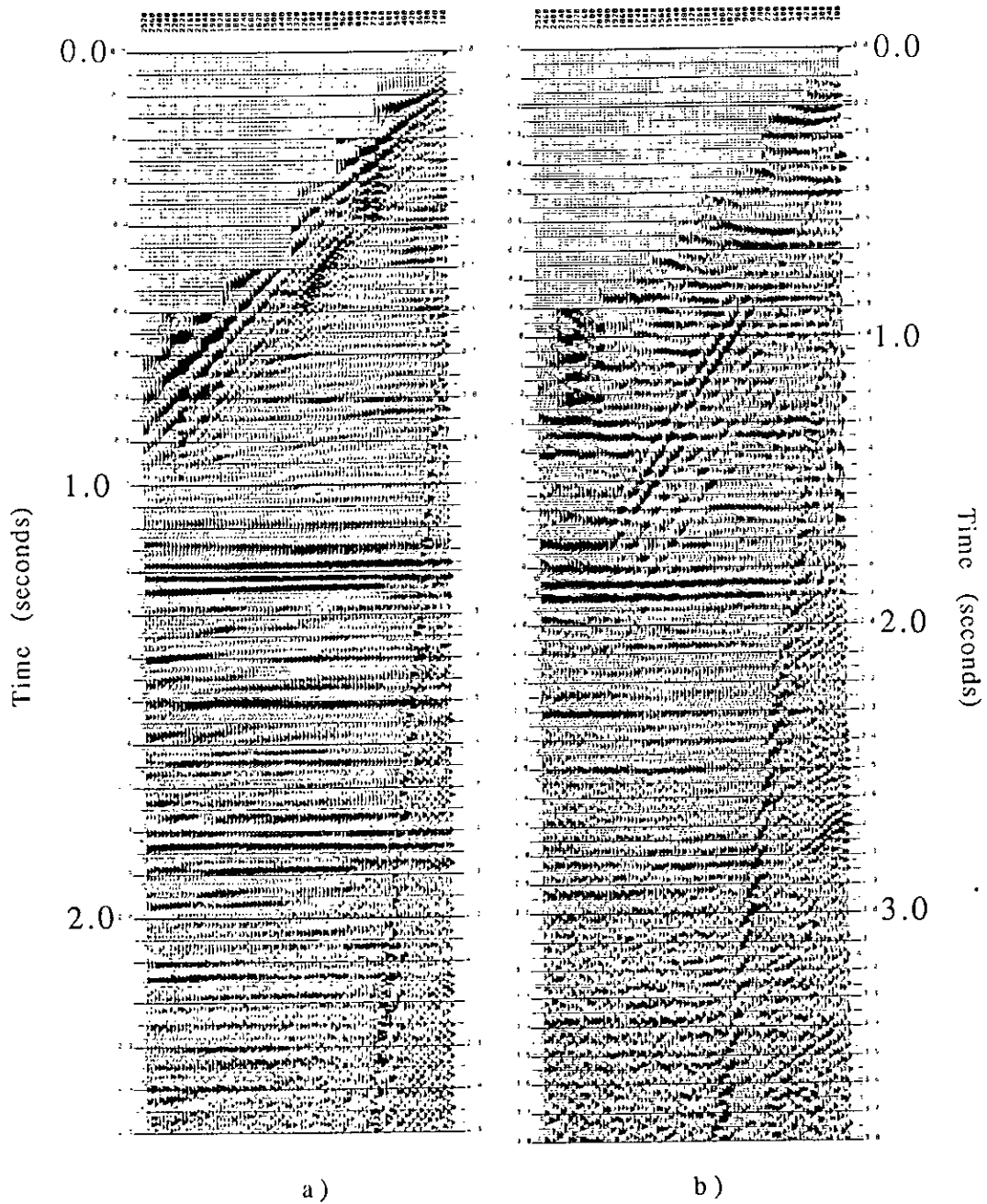


Figure 12. Sample NMO-corrected common-offset stack records for a) the vertical component and b) the radial component data sets.

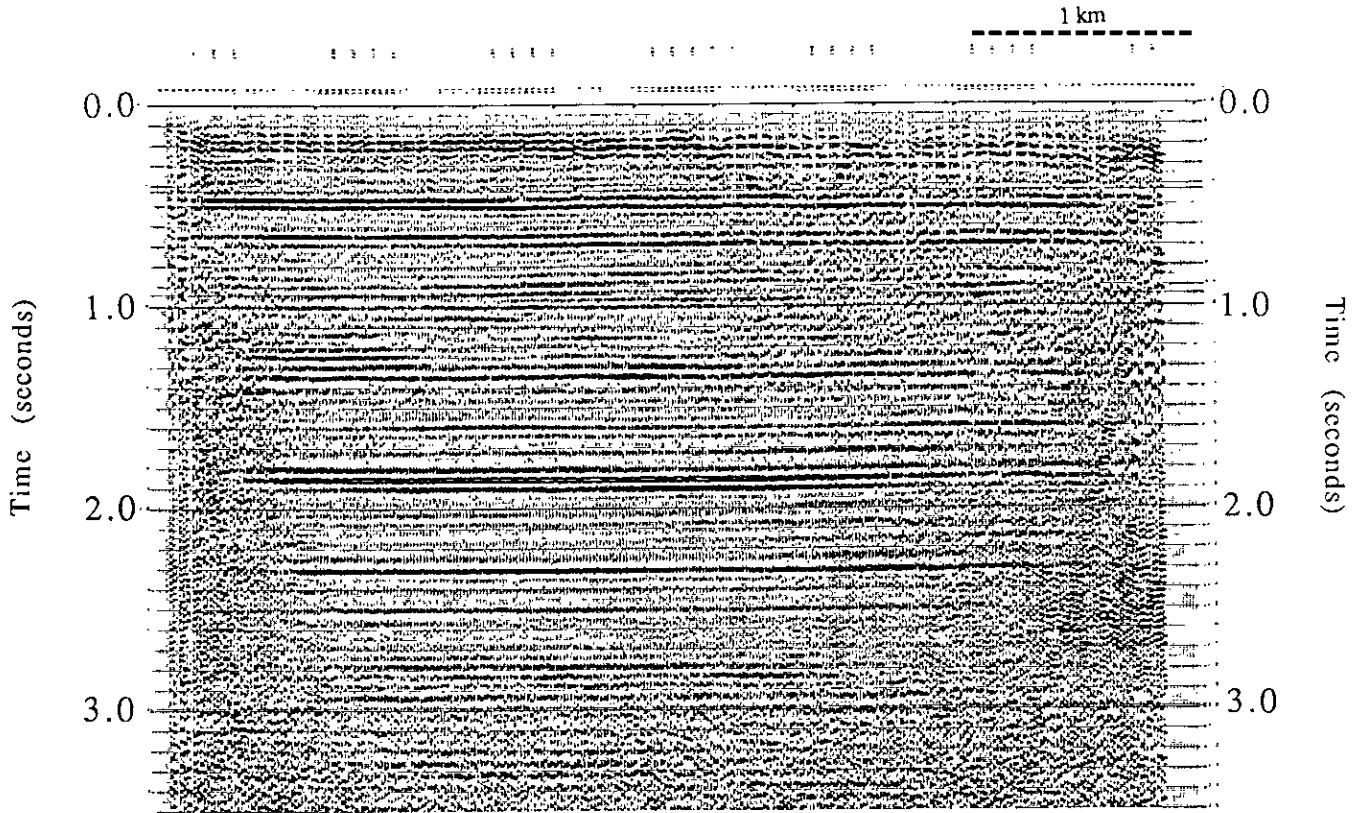


Figure 13. Final stack section for the radial (P-SV) component data.

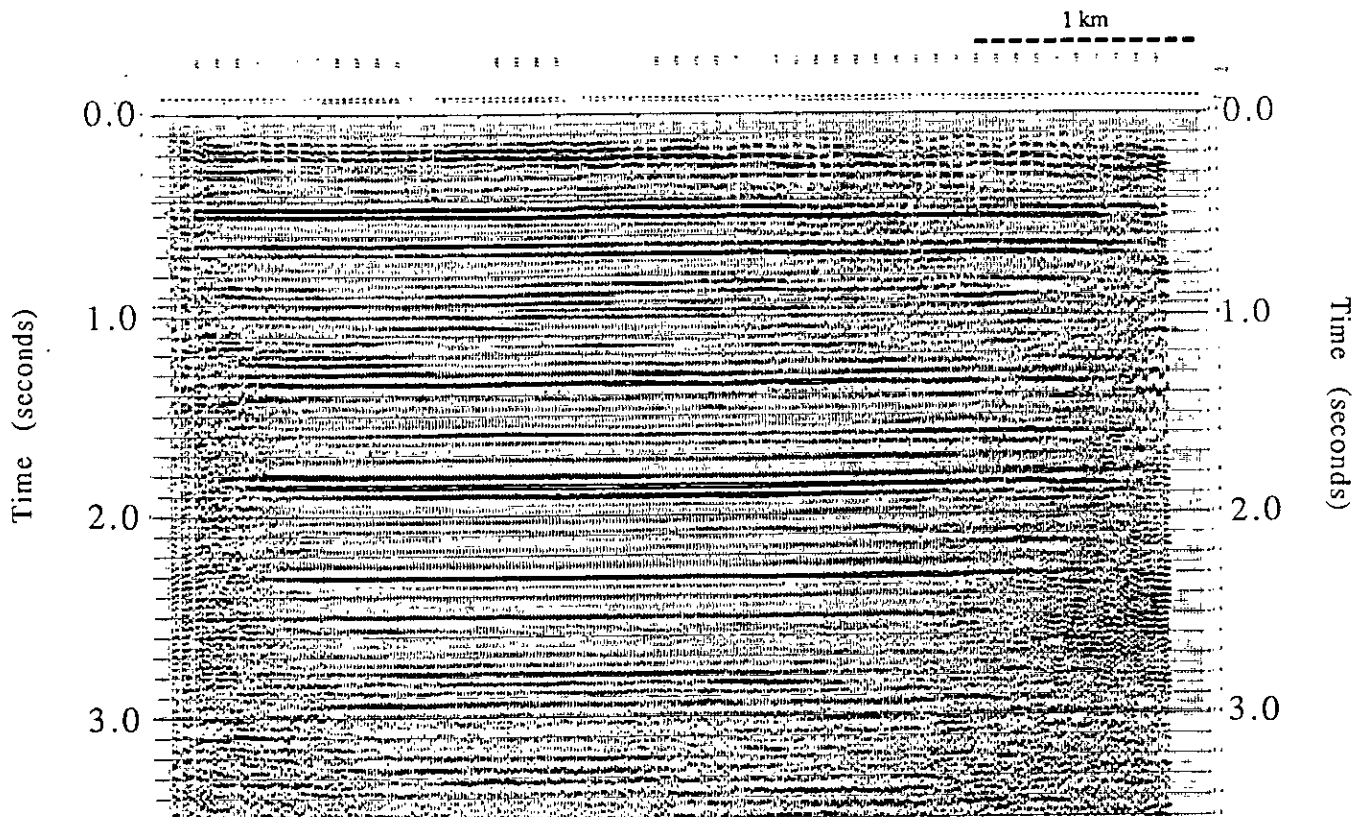
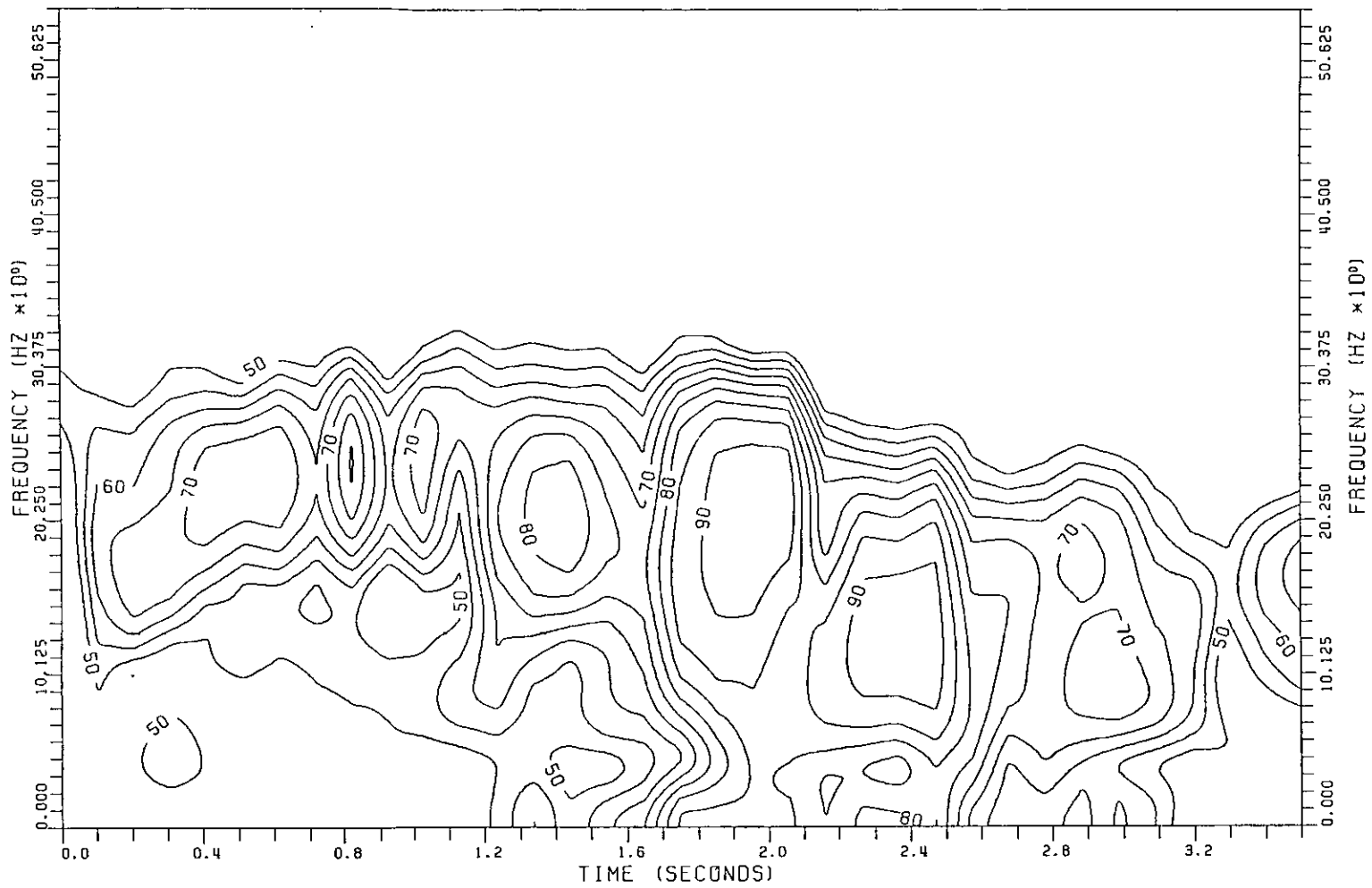


Figure 14. F-K filter applied to the final stack section for the radial (P-SV) component data.

SPECTRA AVERAGED OVER 20 CALCULATIONS  
ENDING WITH IDENT 50000 TRACE 21

MAXIMUM = 0.9415E0

24



CARROT CREEK CCSW01 (RADIAL)  
WINDOW LENGTH = 400 (MS) WINDOW ADVANCE = 100 (MS) STARTING TIME = 0 (MS)  
CONTOURS ARE OF SMOOTHED COHERENCE SPECTRA IN PERCENT

Figure 15. Average time-variant cross-power spectrum between adjacent stack traces of the radial component data.

the velocity of the P-waves would be increased by the presence of water in the low-velocity material, giving an effective depth of the material equal to the depth to the top of the water table. Shear wave energy cannot be transmitted by a fluid, which means the presence of water in the low-velocity material below the water table has little effect on the shear velocity. The shear energy would then be expected to see the full thicknesses and time delays induced by the low-velocity near-surface, while the compressional energy would only see a maximum thickness equal to the depth to the top of the water table. This would result in residual static pockets on the shear data that have no corresponding pockets on the P-wave data, as we see here.

## CONCLUSIONS

The absence of reflection energy in the transverse direction suggests that any velocity anisotropy in the area is either small enough to neglect, or is oriented relative to the line in such a way as to give negligible rotation of SV shear energy propagating in the line plane.

It was found in processing the radial-component data that the source static solution obtained from the vertical component processing was appropriate for the converted shear data. The vertical component receiver statics, however, were not able to properly correct the radial component receivers. From common-receiver surface stacks, residual statics as high as 60 ms were seen to remain in the radial component data. There appears to be no correlation between the size and location of static pockets found on the radial component data to those found on the vertical component data.

Processing of this data set shows that we can produce a stacked section from the radial geophone recording which appears to be converted-wave energy. We have enough signal strength to allow the correlation of events between the P-P and P-SV sections, which allows us to roughly compute the average  $V_p/V_s$  ratio between events. This average  $V_p/V_s$  ratio can then be used for binning the converted-wave data by approximate conversion point. The P-SV section also gives a more obvious indication of the Cardium pool locations than the P-P section by showing a noticeable increase in amplitude.

## PROPOSED RESEARCH

One area of study will be in trying to implement an improved velocity analysis/NMO correction technique. Tessmer and Behle (1988) derive in their paper an NMO equation for converted-wave data that is similar to that used in P-wave processing. They also show that the NMO velocity function for converted-wave data can be combined with the P-wave function to give estimates of the shear-wave interval velocities. They then give examples that show the NMO error due to truncation of higher-order terms to be considerably worse for their converted-wave NMO equation than it is for compressional-wave data at the same offset. A stacking velocity analysis would yield the best-fit hyperbola to the true time-offset curve, which probably would be good enough to correct the data for stacking purposes. The resulting stacking velocity would, however, differ from the true NMO velocity. This means that any estimates of shear-wave interval velocity or  $V_p/V_s$  ratio that we might try to extract from the stacking velocity would be distorted.

Hadley et al., (1988) use a layer-stripping velocity analysis that uses ray-tracing to solve for the NMO time-offset curves for compressional-wave data in areas of complicated geology. A much simpler version of this technique could be used to accurately solve the NMO time-offset equations for converted-wave data. This would allow the assessment of NMO equation truncation effects on shear interval velocity estimation. If the results are significant, then improved velocity analysis and NMO correction using this ray-tracing technique may be useful. A similar technique has been implemented (Harrison, 1989) for

conventional P-wave data processing, and noticeable improvement in interval velocity estimation has been achieved. This suggests that greater improvement might be possible for converted-wave data.

A second area of interest is in the derivation of a method to apply dip-moveout correction (see Hale, 1984) to converted-wave data. The displacement of the P-SV conversion point away from the midpoint complicates the DMO process, and it is not yet known if it can be applied practically.

## ACKNOWLEDGEMENTS

I would like to thank Boyd Exploration and Polyseis Research Inc. for donating the Carrot Creek three-component data set for use by the University of Calgary CREWES group.

## REFERENCES

- Aki, K. and Richards, P.G., 1980, Quantitative Seismology, volume 1: W.H. Freeman and Company, San Francisco.
- Douma, J. and Helbig, K., 1987, What can the polarization of shear waves tell us?: *First Break*, v. 5, 95-104.
- Eaton, D., 1989, Aspects of seismic imaging using P-SV converted waves: this volume.
- Fromm, G., Krey, Th. and Wiest, B., 1985, Static and dynamic corrections, in Dohr, G. Ed., *Seismic Shear Waves: Handbook of Geophysical Exploration*, v. 15a, 191-225.
- Garotta, R., 1985, Observation of shear waves and correlation with P events, in Dohr, G. Ed., *Seismic Shear Waves: Handbook of Geophysical Exploration*, v. 15a, 1-86.
- Hadley, D., Thorsen, J., and Maher, S., 1988, Increasing interpretation accuracy: *Geophysics: The Leading Edge*, Sept. 13-16.
- Hale, D., 1984, Dip-moveout by Fourier transform: *Geophysics*, v. 49, 741-757.
- Harrison, M., 1989, A comparison of exact and conventional normal moveout corrections: Presented at the 1989 Ann. Mtg., Can. Soc. Explor. Geophys.
- Joiner, S.D., 1989, Sedimentology and Ichnology of the Cardium Carrot Creek Field, West Central Alberta, Canada: unpublished thesis, University of Calgary.
- Newman, P., 1973, Divergence effects in a layered earth: *Geophysics*, v. 38, 481-488.
- Pickett, G., 1963, Acoustic character logs and their application in formation evaluation: *J. Petr. Tech.*, v.15, 659-667.
- Schafer, A., 1989, Determination of shear wave statics using converted, refracted waves from a compressional source: this volume.
- Tatham, R.H., 1985, Shear waves and lithology, in Dohr, G. Ed., *Seismic Shear Waves: Handbook of Geophysical Exploration*, v. 15a, 87-133.
- Tessmer, G. and Behle, A., 1988, Common reflection point data-stacking technique for converted waves: *Geophysical Prospecting*, v. 36, 661-688.